PROCEEDINGS, 25th Annual PNOC-EDC Geothermal Conference
Manila Diamond Hotel, Philippines, March 10-11, 2004

CALCULATION OF STEAM AND WATER RELATIVE PERMEABILITIES AT THE GEYSERS AND SALTON SEA GEOTHERMAL RESERVOIRS USING PRODUCTION DATA

Jericho L.P. Reyes and Roland N. Horne

Stanford Geothermal Program, Stanford University, Stanford, CA, U.S.A.

ABSTRACT

The steam and water relative permeabilities at The Geysers and Salton Sea geothermal reservoirs were calculated from available production data. A method was developed to estimate the relative permeability curves using Darcy's Law from mass production rates of steam and water that are available from the DOGGR database. Results show The Geysers behavior approaches the X-curve behavior and Salton Sea behavior approaches Corey curve behavior.

1.0 INTRODUCTION

There are two types of geothermal reservoirs: the vapor-dominated reservoir, where steam is the principal recovery fluid, and the liquid-dominated reservoir, where liquid water is the principal recovery fluid. In both cases, the interaction between these two different phases has been the subject of numerous studies. Most of the experimental activities encounter difficulty due to the phase changes during multiphase flow. An alternative way of determining how these two phases interact while in a state of flow would be very useful in the prediction of the ultimate recovery of the resource. Quantifying this interaction, by calculating the relative permeability of each of the phases, is of particular importance.

The objective of this study was to develop a method to calculate the relative permeability of steam and water by using production data from active geothermal fields.

Knowledge of the relative permeabilities of steam will provide better understanding of the fluid flow interactions in the geothermal reservoir, and this is valuable in estimating the performance of a geothermal field and its capacity for further exploitation.

2.0 BACKGROUND

There have been numerous attempts to characterize the steam and water relative permeability curves both experimentally and theoretically. The main difficulty of such undertakings has been the phase changes that occur in steam and water multiphase flow. A number of experiments have been made to measure steam-water relative permeabilities, such as in air-water (Diomampo, 2001) and water-oil. Current research on steam-water permeability in fractures (Chen et al. 2002), gives us a preliminary insight on the characteristics of the interaction of these two phases with one another.

The two most commonly used functions for relative permeability are the X-curve and the Corey-curve (Corey, 1954). These functions are dependent on phase saturation. The X-curve has a linear relationship with saturation:

$$k_{rl} = S_l \quad (1)$$

$$k_{rg} = S_g \quad (2)$$

where S_l and S_g are the liquid and gas saturation, respectively. The Corey curves relate relative permeability to the irreducible or residual liquid and gas saturation, S_{rl} and S_{rg}:

$$k_{rl} = S^{*4} \quad (3)$$

$$k_{rg} = \left(1 - S^*\right)^2 \left(1 - S^{*2}\right) \quad (4)$$

$$S^* = \left(S_1 - S_{rl}\right) / \left(1 - S_{rl} - S_{rg}\right) \quad (5)$$

Chen et al. (2002) developed a method to compare steam- and air-water transport through fractured media. The main finding was that steam-water flow behavior in fractures is different from that of nitrogen-water flow. Chen et al. (2002) found less phase interference in

steam-water flow, and saw the behavior of the steam-water relative permeabilities behave closer to the X-curve.

The DOGGR Database was made available publicly by the California Division of Oil, Gas and Geothermal Resources. The database contains production histories of, among others, the Geysers and Salton Sea geothermal wells. The data include temperature, pressure and steam and water production rates, and these parameters were used here in this study. The Geysers Geothermal Field, a vapor-dominated reservoir field, is located in Northern California about 130 km north of San Francisco. The Salton Sea Geothermal Field, a liquid-dominated reservoir field, is located in Imperial County in Southern California.

3.0 METHOD

Shinohara (1978) described a method to estimate the steam and water relative permeabilities in geothermal reservoirs. This method was applied to the Wairakei field in New Zealand. This method is very useful, in that it only needs the production flow rate history and the temperature of the reservoir, as well as the ability to evaluate each well separately.

Some of the assumptions of this method include:

(1) The pressure gradient is constant for a short time in each well.
(2) The product of permeability and flowing area is constant in each well.
(3) Fluid flow follows Darcy's Law.

Under these assumptions and from Darcy's law:

$$Q_w = \rho_w \frac{k}{\mu_w} k_{rw} A p' \qquad (6)$$

$$Q_s = \rho_s \frac{k}{\mu_s} k_{rs} A p' \qquad (7)$$

where Q is the mass flowrate, ρ is the density, μ is the dynamic viscosity, k_r is the relative permeability, k is the absolute permeability of the geothermal rock, A is the cross sectional area of flow, and p' is the pressure gradient. The subtitles w and s refer to water and steam respectively.

Dividing Equation 6 by Equation7 gives us:

$$\frac{Q_w}{Q_s} = \frac{\upsilon_w}{\upsilon_s} \frac{k_{rw}}{k_{rs}} \qquad (8)$$

where υ is the kinematic viscosity.

Taking the sum of Equations 6 and 7 gives us:

$$Q = Q_w + Q_s = \left(\rho_w \frac{k_{rw}}{\mu_w} + \rho_s \frac{k_{rs}}{\mu_s} \right) kAp'$$
$$= \left(\frac{k_{rs}}{\upsilon_s} \right) \left[1 + \left(\frac{Q_w}{Q_s} \right) \right] kAp' \qquad (9)$$

where Q is the total of mass production rate of steam and water.

If we assume *kAp'* is constant in each well, then Equation 9 shows that a plot of Q vs. Q_w/Q_s would be almost linear, and we can find the value of *kAp'* from either the intercept or the gradient of the line on the graph. This intercept, where $Q_w/Q_s = 0$, becomes Q*, where:

$$Q^* = \frac{1}{\upsilon_s} kAp' \qquad (10)$$

Because $k_{rs} = 1$ at $Q_w = 0$, then, substituting Equation 10 into Equation 6 and 7,

$$k_{rw} = \left(\frac{\upsilon_w}{\upsilon_s} \right) \left(\frac{Q_w}{Q^*} \right) \qquad (11)$$

and

$$k_{rs} = \frac{Q_s}{Q^*} \qquad (12)$$

Therefore, knowing Q*, we can calculate k_{rs} and k_{rw}, by also knowing Q_w, Q_s, υ_s, and υ_w.

Water saturation can be calculated from

$$S_w = \frac{(1-x)v_w}{(1-x)v_w + xv_w} \qquad (13)$$

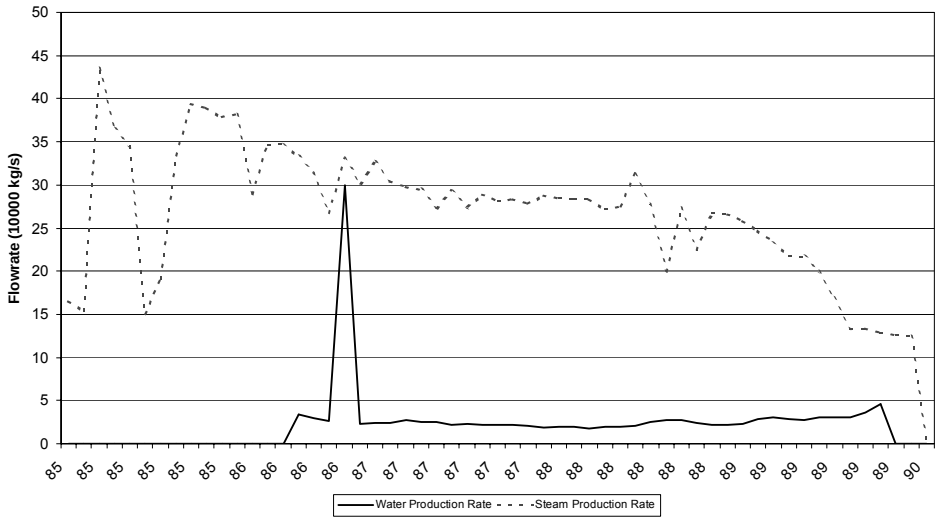

Figure 1. Steam and water production history of Coleman 4-5, The Geyser Geothermal Field.

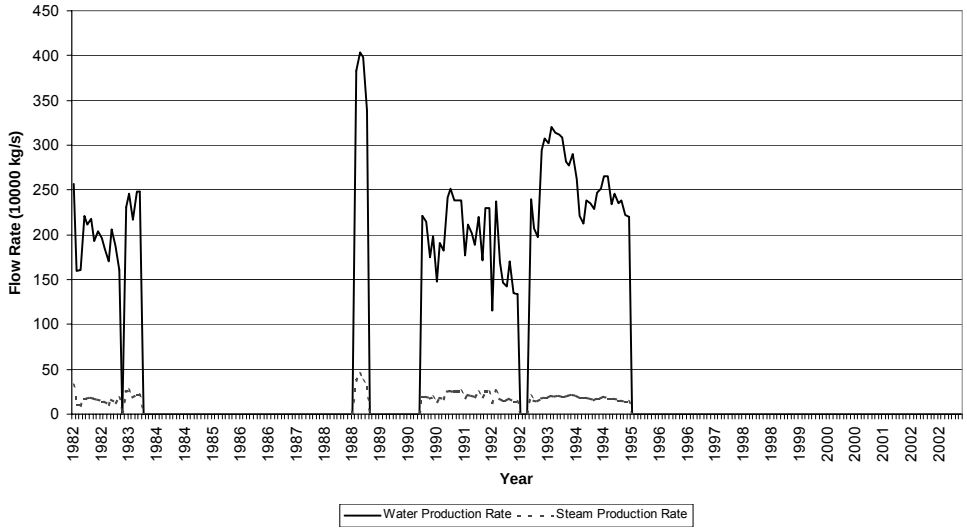

Figure 2. Steam and water production history of IID - 9, Salton Sea Geothermal Field.

where x is the mass fraction of steam and v_w and v_s is the specific volume of water and steam, respectively.

In choosing the wells to use in this study, a couple of issues had to be addressed. First, for the vapor-dominated reservoir, we had to find data that had both steam and water production in order to calculate multiphase properties. Of the 503 wells made available to us from The Geysers, 25 of these wells produced water. Nine wells were ultimately used, as these wells had a sufficient number of readings for the calculation.

Also, the first assumption of Shinohara's method tells us that it is necessary to choose a short time period wherein we can assume a constant pressure gradient during the production of the well. Since production data usually are intermittent in nature and often have periodic fluctuations, we had to find data sets that had significant stable periods. Of the 128 wells documented in the database that belong to the Salton Sea field operated by CalEnergy, we use six wells for our liquid-dominated case.

Figures 1 and 2 are examples of steam and water productions histories from Coleman 4-5, a Geysers well, and IDD – 9, a well from the Salton Sea geothermal field.

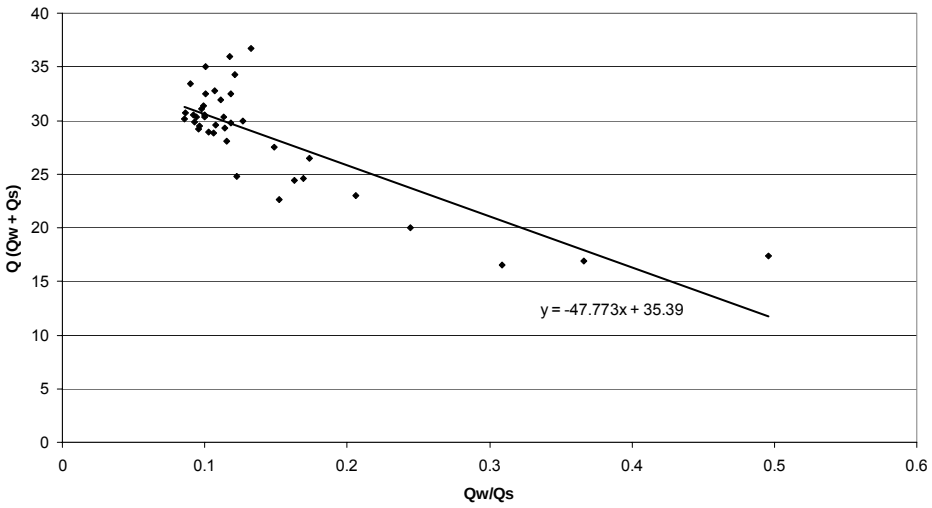

Figure 3. Q vs. Q_w/Q_s to infer Q* for Coleman 4-5, The Geysers Geothermal Field.

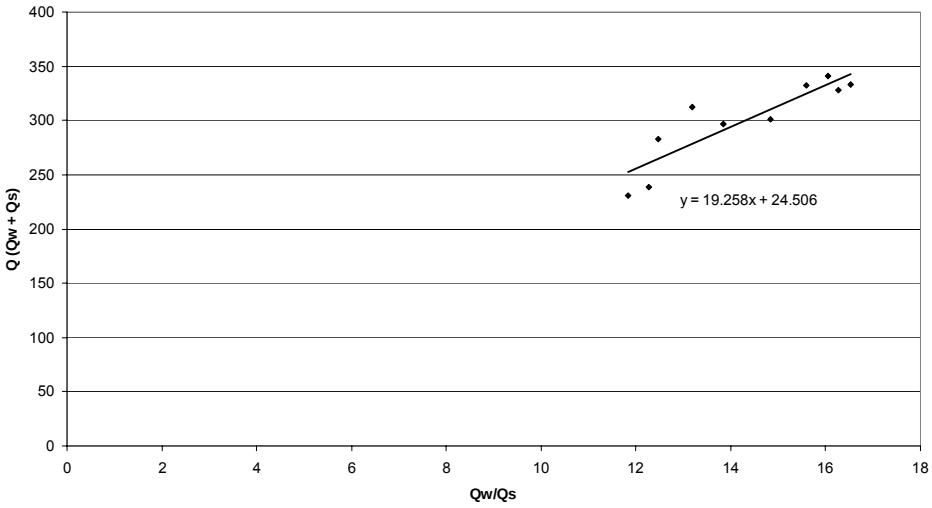

Figure 4. Q vs. Q_w/Q_s to infer Q* for IID - 9, Salton Sea Geothermal Field.

Well IDD-9 (Fig. 2) from Salton Sea had zero production for much of its history. We therefore chose an interval that we can assume to have a constant roughly pressure gradient. For this work we chose a mid-1990 to late-1992 interval.

Choosing the time interval for the vapor-dominated well is much easier. We chose from the mid-1986 to 1989 readings. We try to omit extreme readings from our analysis; therefore the spike seen in 1986-1987 was not part of the range. For this work, we took a mid-1987 to 1989 interval.

Figures 3 and 4 show the Q vs Q_w/Q_s graphs for Coleman 5-5 and IDD – 9, respectively. The value of Q* is inferred from the y-intercept value from the linear fit to the graph. Table 1 shows the Q* inferred from all the wells used in the study.

If we compare the Q* values between the Geysers wells and the Salton Sea wells, we can see that the Geysers's Q*values are smaller than the Salton Sea values. Also, the Geysers's Q* values are near each other. This is an extension of the second assumption made by Shinohara in developing his method. Not only is kAp' constant in a well, wells that are near each

Table 1. Inferred Q* values for the Geysers and Salton Sea Geothermal Field Wells.

Name of Well	*Q**
Geysers Wells	
Coleman 4-5	35.39
Coleman 5-5	35.649
Coleman 3-5	24.186
Francisco 2-5	24.182
Coleman 1A-5	24.09
Thorne 6	33.59
Thorne 1	17.384
Francisco 5-5	23.52
CA-5636 6.8E-20	27.868
Salton Sea Wells	
IID – 9	100
Sinclair 20	75
Vonderahe 1	437.56
Sinclair 10	298.62
Elmore 100	200
Sinclair 11	256.5

other or belong to the same geothermal field also have similar kAp' values. Since the wells in a certain geothermal field mainly have the same k values, and to a certain extent, A and p', then our inferred values are consistent with each other. The Salton Sea's values have a wider range of values, but are generally in the same larger magnitude compared to the Geysers'.

To correctly evaluate the kinematic viscosities and mass production rates of the steam and water, we must infer the bottomhole conditions of the wells, as this reflects the true flowing conditions of the well. We made temperature corrections based on the documented depths of the wells.

4.0 RESULTS AND DISCUSSION

We can now use Equations 6 and 7 to calculate the relative permeabilities of steam and water. Figures 5 and 6 shows us a plot of relative permeability with water saturation for the Geysers and Salton Sea geothermal wells, respectively. Note that these graphs are plotted against the mobile saturation, S*, as defined by Equation 5. The mobile saturation excludes the immobile water and steam fractions.

Figure 5 shows us The Geysers relative permeability plot. Because The Geysers is vapor-dominated reservoir, we expected the low water saturation values that are calculated. Figure 6, the Salton Sea examples, shows us a larger range for water saturation, with a maximum at around 0.25. Even with a vapor-dominated reservoir, we see that, volumetrically, the steam saturation values still dominate, even if, by mass, water production has the larger portion.

We try to see the general trend of the relative permeability curves by plotting both well samples into Figure 7.

We see that the relative permeability values for the vapor-dominated and liquid-dominated samples are only partially consistent with each other. For the relative permeability for steam, the Geysers calculation gives us a sharp drop in k_{rs} at small values of S_w. We then see a plateau of values approaching $S_w = 0.1$ from the Salton Sea values. For the relative permeability of water, we see a more constant and stable rise as the water saturation also rises. The steepness of the rise for both set of well samples are consistent.

To compare the relative permeability values calculated with the two most commonly assumed models of relative permeabilities, namely Corey and X curves, we plot the computed k_{rw} and k_{rs} values with these model curves. Figures 8 and 9 show the plots k_{rw} vs. k_{rs} of for the Geysers and Salton Sea well samples, respectively.

For The Geysers samples, we see that the relative permeability follows the Corey-curve relationship. We see, as we saw from Figure 7, that k_{rs} drops sharply at earlier values, this time for k_{rw}. Figure 8 shows the Salton Sea values are more in the middle of the X-curve and Corey-curve. We also see that k_{rs} increases more slowly compared to the rise of k_{rw}. As this happens, the curve goes from the X-curve and approaches the Corey-curve.

In terms of phase interference, we see that at low water saturation, steam relative permeability drops sharply, suggesting that the presence of water greatly interferes with the flow of steam. The water did not seem to be affected by the presence of the steam, at least with $S_w < 0.2$, as the increase in relative permeability of water is stable and almost constant. However, the behavior still exhibits more interference than the X-curve, with an almost 1:2 ratio between k_{rw} and S_w.

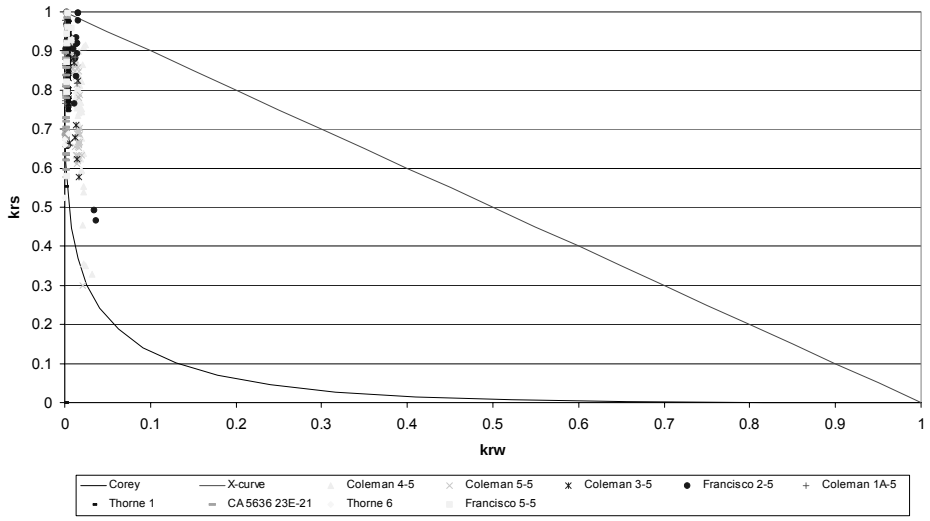

Figure 5. Plot of relative permeability curves against water saturation for The Geysers Geothermal Field.

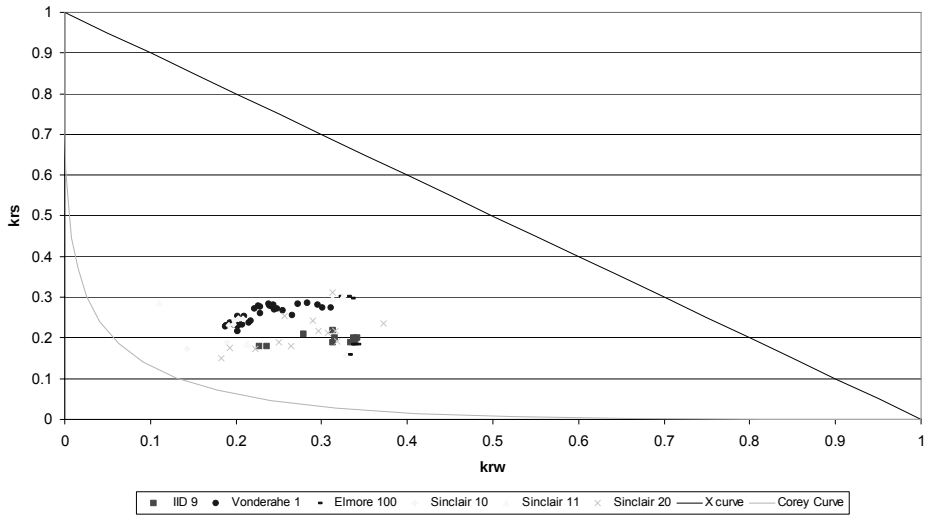

Figure 6. Plot of relative permeability curves against water saturation for the Salton Sea Geothermal Field.

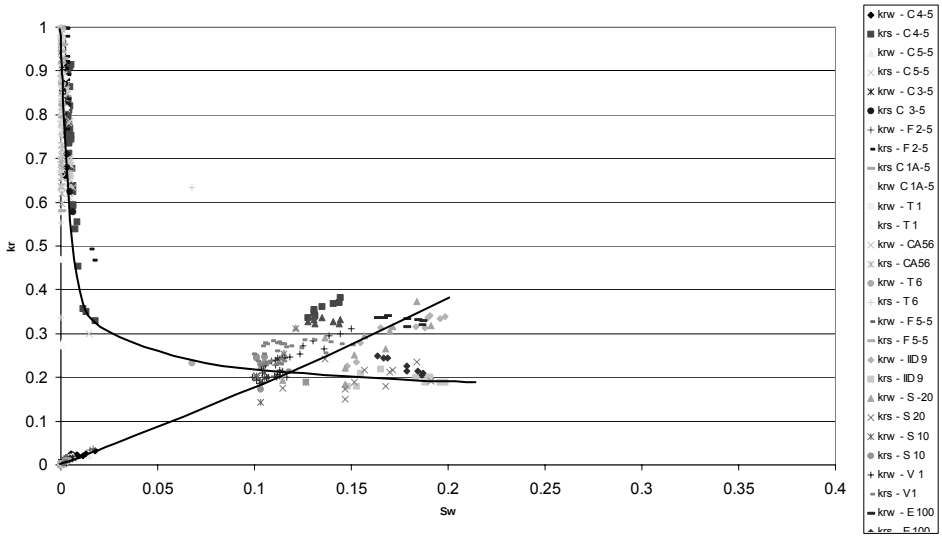

Figure 7. Plot of relative permeability curves against water saturation for The Geysers and Salton Sea Geothermal Fields.

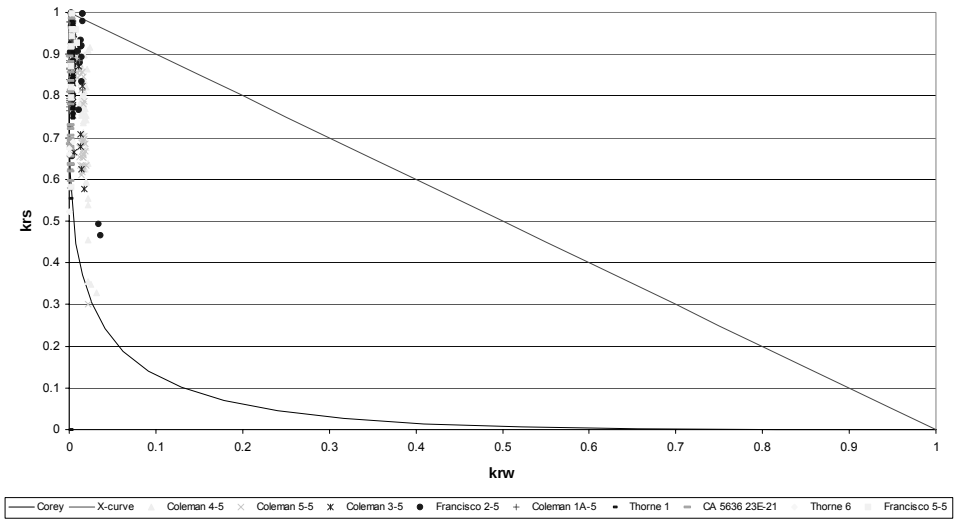

Figure 8. Plot of k_{rw} vs. k_{rs} for The Geyser Geothermal Field, with the Corey and X-curves.

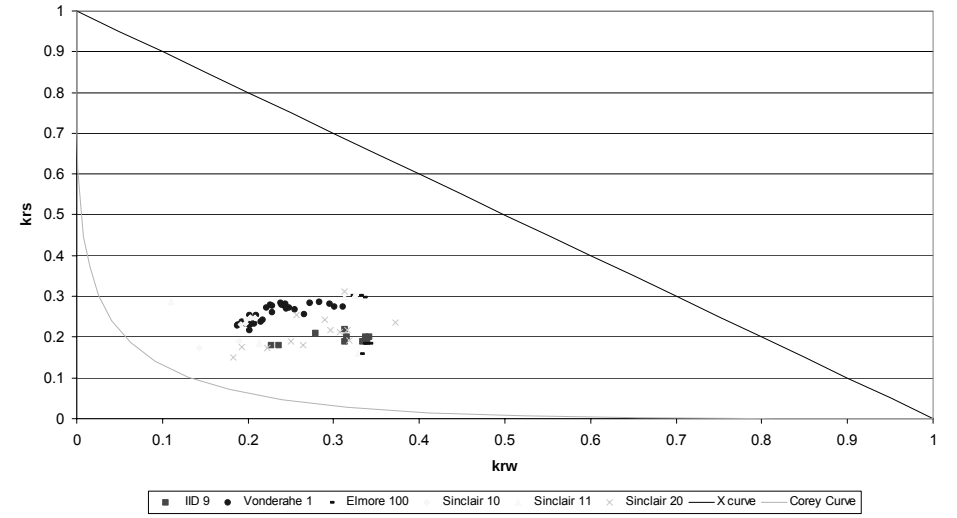

Figure 9. Plot of k_{rw} vs. k_{rs} for the Salton Sea Geothermal Field, with the Corey and X-curves.

We plot Figures 8 and 9 again, this time with logarithmic axes. Figures 10 and 11 plots these graphs for the Geysers and Salton Sea well samples, respectively.

We see from these two graphs that the calculated values are in the middle of the X- and Corey-curves. Although the relationship we saw in Figure 8 cannot be seen in Figure 10 because of the difference in scale, we see a somewhat similar relationship between Figures 10 and 11, wherein the curve approaches the X-curve as S_w increases.

5.0 CONCLUSIONS

a. We can obtain the relative permeabilities from the production flow rate history and bottomhole temperature

b. There is a sharp decline in the relative permeability of steam at small values of mobile water saturation, and this decline moderates as the saturation increases

c. The relative permeability of water has a more stable increase compared to the relative permeability of steam.

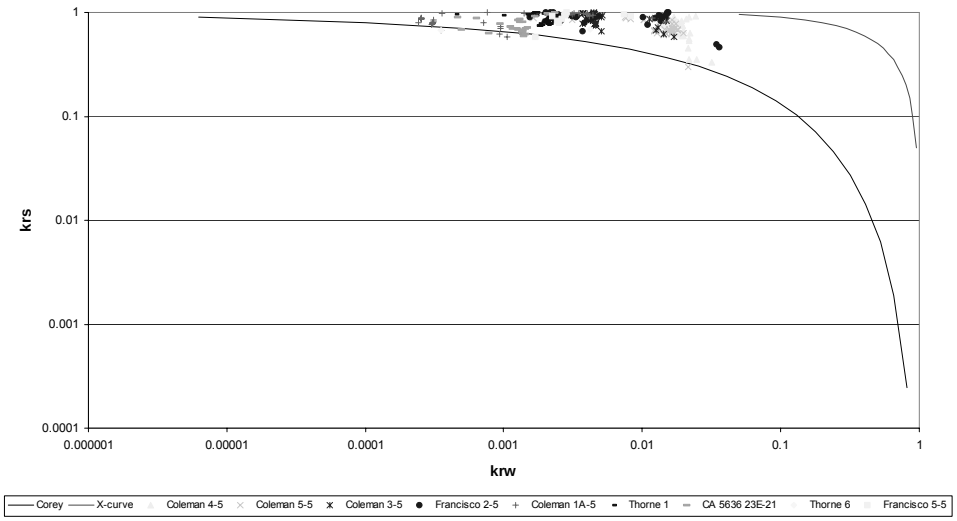

Figure 10. Logarithmic Plot of k_{rw} vs k_{rs} for the Salton Sea Geothermal Field, with the Corey and X-curves.

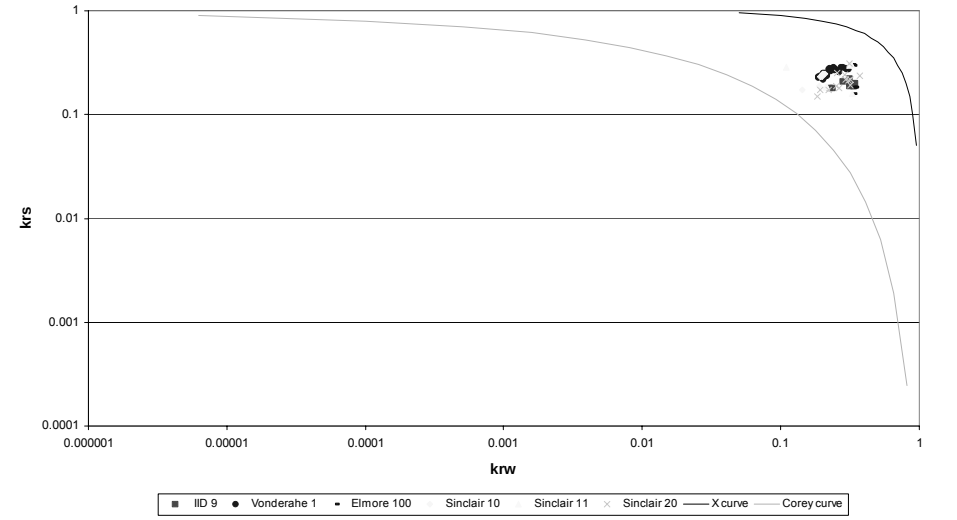

Figure 11. Logarithmic Plot of k_{rw} vs k_{rs} for the Salton Sea Geothermal Field, with the Corey and X-curves.

d. The values of relative permeability follow the X-curve at small water saturation values in the Geysers field, and then approaches the Corey-curve as the water saturation increases in the Salton Sea Field.

REFERENCES

Chen, C.-Y., Diomampo, G., Li, K. and Horne, R.N. (2002). Steam-water relative permeability in fractures. Geothermal Resources Council Transactions, vol.26, 87-94.

Corey, A.T. (1954). The interrelations between gas and oil relative permeabilities. Producers Monthly, vol. 19, 38-41.

Diomampo, G. (2001). Relative permeability through fractures. MS thesis, Stanford University, Stanford, California.

Shinohara, K. (1978). Calculation and use of steam/water relative permeabilities in geothermal reservoirs. MS thesis, Stanford University, Stanford, California.